Microfluidic device for continuous single cells analysis via Raman spectroscopy enhanced by integrated plasmonic nanodimers

Microfluidic device for continuous single cells analysis via Raman spectroscopy enhanced by integrated plasmonic nanodimers

Gerardo Perozziello,[1] Patrizio Candeloro,[1] Antonio De Grazia,[2] Francesco Esposito,[1] Marco Allione,[2] Maria Laura Coluccio,[2] Rossana Tallerico,[1] Immanuel Valpapuram,[2] Luca Tirinato,[2] Gobind Das,[2] Andrea Giugni,[2] Bruno Torre,[2] Pierangelo Veltri,[3] Ulrich Kruhne,[4] Giuseppe Della Valle,[5] and Enzo Di Fabrizio[2,*]

[1]*Department of Experimental and Clinical Medicine, BioNEM lab, University "Magna Graecia" of Catanzaro, 88100 Catanzaro, Italy*

[2]*Division of Physical Science and Engineering and Biological and Environmental Sciences and Engineering, SMILEs lab, King Abdullah University of Science and Technology (KAUST), Thuwal, Saudi Arabia*

[3]*Department of Surgical and Medical Science, University "Magna Graecia" of Catanzaro, 88100 Catanzaro, Italy*

[4]*Department of Chemical and Biochemical Engineering, Technical University of Denmark (DTU), 2800 Kgs. Lyngby, Denmark*

[5]*Department of Physics, Politecnico di Milano, Istituto di Fotonica e Nanotecnologie – CNR, I-20133 Milano, Italy*

[*]*Enzo.difabrizio@kaust.edu.sa*

Abstract: In this work a Raman flow cytometer is presented. It consists of a microfluidic device that takes advantages of the basic principles of Raman spectroscopy and flow cytometry. The microfluidic device integrates calibrated microfluidic channels– where the cells can flow one-by-one –, allowing single cell Raman analysis. The microfluidic channel integrates plasmonic nanodimers in a fluidic trapping region. In this way it is possible to perform Enhanced Raman Spectroscopy on single cell. These allow a label-free analysis, providing information about the biochemical content of membrane and cytoplasm of the each cell. Experiments are performed on red blood cells (RBCs), peripheral blood lymphocytes (PBLs) and myelogenous leukemia tumor cells (K562).

OCIS codes: (130.0130) Integrated optics; (170.1530) Cell analysis.

References and links

1. G. M. Whitesides, "The origins and the future of microfluidics," Nature **442**(7101), 368–373 (2006).
2. G. Simone and G. Perozziello, "UV/Vis visible optical waveguides fabricated using organic-inorganic nanocomposite layers," J. Nanosci. Nanotechnol. **11**(3), 2057–2063 (2011).
3. F. De Angelis, A. Pujia, C. Falcone, E. Iaccino, C. Palmieri, C. Liberale, F. Mecarini, P. Candeloro, L. Luberto, A. de Laurentiis, G. Das, G. Scala, and E. Di Fabrizio, "Water soluble nanoporous nanoparticle for in vivo targeted drug delivery and controlled release in B cells tumor context," Nanoscale **2**(10), 2230–2236 (2010).
4. A. A. Yu, T. Savas, S. Cabrini, E. Difabrizio, H. I. Smith, and F. Stellacci, "High resolution printing of DNA feature on poly(methyl methacrylate) substrates using supramolecular nano-stamping," J. Am. Chem. Soc. **127**(48), 16774–16775 (2005).
5. Y. Zhang, S. Park, S. Yang, and T. H. Wang, "An all-in-one microfluidic device for parallel DNA extraction and gene analysis," Biomed. Microdevices **12**(6), 1043–1049 (2010).
6. G. Keramas, G. Perozziello, O. Geschke, and C. B. V. Christensen, "Development of a multiplex microarray microsystem," Lab Chip **4**(2), 152–158 (2004).
7. K. Liu and Z. H. Fan, "Thermoplastic microfluidic devices and their applications in protein and DNA analysis," Analyst (Lond.) **136**(7), 1288–1297 (2011).
8. J. Wu, X. Z. Wu, T. Huang, and J. Pawliszyn, *Analysis of Proteins by CE, CIEF, and Microfluidic Devices with Whole-Column-Imaging Detection*, M. A. Strege, A. L. Lagu, eds. (Humana Press, 2004).
9. G. Perozziello, P. Candeloro, F. Gentile, M. L. Coluccio, M. Tallerico, A. De Grazia, A. Nicastri, A. M. Perri, E. Parrotta, F. Pardeo, R. Catalano, G. Cuda, and E. Di Fabrizio, "A microfluidic dialysis device for complex biological mixture SERS analysis," Microelectron. Eng. **144**, 37–41 (2015).
10. H. C. Tekin, C. Scherz, and M. A. M. Gijs, "Microfluidic device for analysis of protein biomarkers using magnetic bead surface coverage detection," in *Proceedings of the 15th International Conference on Miniaturized Systems for Chemistry and Life Sciences* (MicroTAS, 2011).

#252075 Received 16 Oct 2015; revised 26 Nov 2015; accepted 27 Nov 2015; published 11 Dec 2015

11. G. Perozziello, P. Candeloro, F. Gentile, A. Nicastri, A. Perri, M. L. Coluccio, A. Adamo, F. Pardeo, R. Catalano, E. Parrotta, H. D. Espinosa, G. Cuda, and E. Di Fabrizio, "Microfluidics & nanotechnology: towards fully integrated analytical devices for the detection of cancer biomarkers," RSC Advances **4**(98), 55590–55598 (2014).
12. G. Perozziello, R. La Rocca, G. Cojoc, C. Liberale, N. Malara, G. Simone, P. Candeloro, A. Anichini, L. Tirinato, F. Gentile, M. L. Coluccio, E. Carbone, and E. Di Fabrizio, "Microfluidic devices modulate tumor cell line susceptibility to NK cell recognition," Small **8**(18), 2886–2894 (2012).
13. G. Simone and G. Perozziello, "Ca2+ Mediates the Adhesion of Breast Cancer Cells in Self-Assembled Multifunctional Microfluidic Chip prepared with Carbohydrate Beads," Micro Nanosyst. **2**(4), 261–268 (2010).
14. G. Simone, G. Perozziello, E. Battista, F. De Angelis, P. Candeloro, F. Gentile, N. Malara, A. Manz, E. Carbone, P. Netti, and E. Di Fabrizio, "Cell rolling and adhesion on surfaces in shear flow. A model for an antibody-based microfluidic screening system," Microelectron. Eng. **98**, 668–671 (2012).
15. G. Perozziello, G. Simone, N. Malara, R. La Rocca, R. Tallerico, R. Catalano, F. Pardeo, P. Candeloro, G. Cuda, E. Carbone, and E. Di Fabrizio, "Microfluidic biofunctionalisation protocols to form multi-valent interactions for cell rolling and phenotype modification investigations," Electrophoresis **34**(13), 1845–1851 (2013).
16. G. Perozziello, R. Catalano, M. Francardi, E. Rondanina, F. Pardeo, F. De Angelis, N. Malara, P. Candeloro, G. Morrone, and E. Di Fabrizio, "A microfluidic device integrating plasmonic nanodevices for Raman spectroscopy analysis on trapped single living cells," Microelectron. Eng. **111**, 314–319 (2013).
17. Y. Zheng, J. Nguyen, C. Wang, and Y. Sun, "Electrical measurement of red blood cell deformability on a microfluidic device," Lab Chip **13**(16), 3275–3283 (2013).
18. J. M. Kwan, Q. Guo, D. L. Kyluik-Price, H. Ma, and M. D. Scott, "Microfluidic analysis of cellular deformability of normal and oxidatively damaged red blood cells," Am. J. Hematol. **88**(8), 682–689 (2013).
19. V. Faustino, D. Pinho, T. Yaginuma, R. C. Calhelha, I. C. Ferreira, and R. Lima, "Extensional flow-based microfluidic device: deformability assessment of red blood cells in contact with tumor cells," Biochip J. **8**(1), 42–47 (2014).
20. F. Gentile, G. Das, M. L. Coluccio, F. Mecarini, A. Accardo, L. Tirinato, R. Tallerico, G. Cojoc, C. Liberale, P. Candeloro, P. De Cuzzi, F. De Angelis, and E. Di Fabrizio, "Ultra low concentrated molecular detection using super hydrophobic surface based biophotonic devices," Microelectron. Eng. **87**(5), 798–801 (2010).
21. F. De Angelis, M. Malerba, M. Patrini, E. Miele, G. Das, A. Toma, R. P. Zaccaria, and E. Di Fabrizio, "3D hollow nanostructures as building blocks for multifunctional plasmonics," Nano Lett. **13**(8), 3553–3558 (2013).
22. H. Wu, J. V. Volponi, A. E. Oliver, A. N. Parikh, B. A. Simmons, and S. Singh, "In vivo lipidomics using single-cell Raman spectroscopy," Proc. Natl. Acad. Sci. U.S.A. **108**(9), 3809–3814 (2011).
23. T. Ichimura, L. D. Chiu, K. Fujita, S. Kawata, T. M. Watanabe, T. Yanagida, and H. Fujita, "Visualizing cell state transition using Raman spectroscopy," PLoS One **9**(1), e84478 (2014).
24. H. M. Shapiro, *Practical Flow Cytometry* (John Wiley & Sons Inc, 2005).
25. M. G. Ormerod and D. Novo, "Flow cytometry: a basic introduction", MG Ormerod, (2008).
26. M. J. Pelletier, "Quantitative analysis using Raman spectrometry," Appl. Spectrosc. **57**(1), 20–42 (2003).
27. E. B. Hanlon, R. Manoharan, T. W. Koo, K. E. Shafer, J. T. Motz, M. Fitzmaurice, J. R. Kramer, I. Itzkan, R. R. Dasari, and M. S. Feld, "Prospects for in vivo Raman spectroscopy," Phys. Med. Biol. **45**(2), R1–R59 (2000).
28. P. J. Caspers, G. W. Lucassen, R. Wolthuis, H. A. Bruining, and G. J. Puppels, "In vitro and in vivo Raman spectroscopy of human skin," Biospectroscopy **4**(5), S31–S39 (1998).
29. N. Colthup, *Introduction to infrared and Raman spectroscopy*, (Amsterdam: Elsevier, 2012).
30. D. Cojoc, V. Garbin, E. Ferrari, L. Businaro, F. Romanato, and E. D. Fabrizio, "Laser trapping and micro-manipulation using optical vortices," Microelectron. Eng. **78**, 125–131 (2005).
31. M. Chirumamilla, A. Toma, A. Gopalakrishnan, G. Das, R. P. Zaccaria, R. Krahne, E. Rondanina, M. Leoncini, C. Liberale, F. De Angelis, and E. Di Fabrizio, "3D Nanostar Dimers with a Sub-10-nm Gap for Single-/Few-Molecule Surface-Enhanced Raman Scattering," Adv. Mater. **26**(15), 2353–2358 (2014).
32. F. De Angelis, C. Liberale, M. L. Coluccio, G. Cojoc, and E. Di Fabrizio, "Emerging fabrication techniques for 3D nano-structuring in plasmonics and single molecule studies," Nanoscale **3**(7), 2689–2696 (2011).
33. M. L. Coluccio, F. Gentile, G. Das, A. Nicastri, A. M. Perri, P. Candeloro, G. Perozziello, R. Proietti Zaccaria, J. S. Gongora, S. Alrasheed, A. Fratalocchi, T. Limongi, G. Cuda, and E. Di Fabrizio, "Detection of single amino acid mutation in human breast cancer by disordered plasmonic self-similar chain," Sci. Adv. **1**(8), e1500487 (2015).
34. M. L. Coluccio, F. Gentile, M. Francardi, G. Perozziello, N. Malara, P. Candeloro, and E. Di Fabrizio, "Electroless Deposition and Nanolithography Can Control the Formation of Materials at the Nano-Scale for Plasmonic Applications," Sensors (Basel) **14**(4), 6056–6083 (2014).
35. L. Lu, X. L. Xu, W. T. Liang, and H. F. Lu, "Raman analysis of CdSe/CdS core-shell quantum dots with different CdS shell thickness," J. Phys. Condens. Matter **19**(40), 406221 (2007).
36. S. V. Zhukovsky, T. Ozel, E. Mutlugun, N. Gaponik, A. Eychmüller, A. V. Lavrinenko, H. V. Demir, and S. V. Gaponenko, "Hyperbolic metamaterials based on quantum-dot plasmon-resonator nanocomposites," Opt. Express **22**(15), 18290–18298 (2014).
37. A. Balandin, K. L. Wang, N. Kouklin, and S. Bandyopadhyay, "Raman spectroscopy of electrochemically self-assembled CdS quantum dots," Appl. Phys. Lett. **76**(2), 137–139 (2000).
38. G. Perozziello, F. Bundgaard, and O. Geschke, "Fluidic interconnections for microfluidic systems: a new integrated fluidic interconnection allowing plug 'n'play functionality," Sens. Actuators B Chem. **130**(2), 947–953 (2008).
39. W. D. Callister and D. G. Rethwisch, *Materials Science and Engineering: An Introduction*, (John Wiley & Sons Inc., 2007).

#252075 Received 16 Oct 2015; revised 26 Nov 2015; accepted 27 Nov 2015; published 11 Dec 2015

40. B. R. Wood, P. Caspers, G. J. Puppels, S. Pandiancherri, and D. McNaughton, "Resonance Raman spectroscopy of red blood cells using near-infrared laser excitation," Anal. Bioanal. Chem. **387**(5), 1691–1703 (2007).
41. A. Bankapur, E. Zachariah, S. Chidangil, M. Valiathan, and D. Mathur, "Raman Tweezers Spectroscopy of Live, Single Red and White Blood Cells," PLoS One **5**(4), e10427 (2010).
42. R. Tallerico, M. Todaro, S. Di Franco, C. Maccalli, C. Garofalo, R. Sottile, C. Palmieri, L. Tirinato, P. N. Pangigadde, R. La Rocca, O. Mandelboim, G. Stassi, E. Di Fabrizio, G. Parmiani, A. Moretta, F. Dieli, K. Kärre, and E. Carbone, "Human NK Cells Selective Targeting of Colon Cancer-Initiating Cells: A Role for Natural Cytotoxicity Receptors and MHC Class I Molecules," J. Immunol. **190**(5), 2381–2390 (2013).
43. Y. H. Ong, M. Lim, and Q. Liu, "Comparison of principal component analysis and biochemical component analysis in Raman spectroscopy for the discrimination of apoptosis and necrosis in K562 leukemia cells," Opt. Express **20**(20), 22158–22171 (2012).

1. Introduction

In the field of cell biology, microfluidics has evolved as a relevant technology. This interdisciplinary discipline focuses on the transport, manipulation and analysis of small amounts of liquids, cells and particles. Microfluidic devices have been exploited in several laboratories for their evident advantages such as, the use of small volumes of fluids. Moreover, these devices guarantee portability, high control of the flow conditions, parallel transport, cost reduction etc [1, 2]. There are many examples in the literature of microfluidic devices and nanotechnologies [3] used for analytical purposes. These have been developed for DNA detection [4–6]; for protein analysis [7–9] and biomarkers [10, 11]; for discriminating healthy by tumor cells [12, 13]; for phenotypes cell screening [14, 15]; for mechanical stress investigation [16] and their deformability [17–19].

Among these technologies we developed a new microfluidic device capable of analyzing the composition of a single cell at a subcellular level thanks to integrated plasmonic nanodimers and Raman spectroscopy. This vibrational spectroscopy allows fast and multiparametric analysis of single cells, producing spectra which can be considered as a fingerprint of the cell. Moreover, it is a non-invasive technique useful to examine biological samples, since water bands can be easily subtracted from the resulted spectra [20–23]. Generally, when Raman spectroscopy is performed on a big number of cells, it is difficult to track them. Moreover, a possible movement of the cell during the analysis has to be taken into account.

The present microfluidic device is composed by two calcium fluoride slides among which a photosensitive resist is placed. The device, consisting of five through-channels integrating a microfluidic trap, is fabricated by using photolithography. The trap is realized by means of a simple volumetric constriction of the channels. Flowing cells in the microchannel can be blocked at each trap where Raman spectroscopy can be performed on each individual cell. A similar mechanism is followed in fluorescent flow cytometry [24, 25]. In that case, an appropriate label preparation of the cells is needed prior to the fluorescence analysis. Raman spectroscopy, on the other hand, is a label free technique and no pre-treatment of the sample is needed [26–29]. However, Raman Spectroscopy requires that the minimum acquisition time is in the range of few seconds for each spectrum. Therefore the device integrates a microfluidic trap with nested plasmonic nanodimers [30]. In particular, the plasmonic nanodevice allows an enhanced Raman scattering that increases the sensitivity and the spectroscopic information [31–34] regarding both the cellular membrane and the cytoplasm of each cell. In the last years, several groups have shown different approaches to enhance Raman signals or more in general luminescent outputs like those working within the field of colloidal photonics where quantum dots are used for such a purpose [35, 36]. Nanodimers are equivalent to quantum dots used to enhance Raman outputs. The local field generated by dimers can be obtained even by colloidal synthesis [37]. These devices are based on the amplification of the electromagnetic field due to the polarization of the local electric field and resonance effects between the gap of the nanodimers. In this way, it is possible to obtain a field localization that depends on the size of the gap (approximately 5-10 nm).

#252075 Received 16 Oct 2015; revised 26 Nov 2015; accepted 27 Nov 2015; published 11 Dec 2015

2. Materials and methods

The working principle of the present device is based on the use of a microfluidic trap integrated with a plasmonic Raman enhancer. The device is interfaced with gaskets that protect the fragile chip from mechanical stresses and seals the microchannels to an external frame integrating external tubes. These are then connected to a syringe pump system (Harvard Apparatus) allowing to handle the biological sample and drive it into the microfluidic channels. In such a device, ideally, every kind of cell can be analyzed by adjusting properly the sizes of the channels and the traps. The present device can be used in different modes: - we can move the same cell forth and back in the trap by changing direction of the flow so that we can take measurements on different portion of the same cell [16]; - we can take one single measurement on a cell sitting on the nanodimers in the field of view, and getting the information from one single cell membrane. The measurements from single cells of the same type can be also integrated together (which is what it is shown in the presented work). This procedure can be repeated in several different cells of the same type; - we can perform micro-RAMAN by using objectives with higher NA, in this case the measurement can be used to search for specific information about the cell membrane and cytoplasm. The microfluidic device is characterized by analyzing sample of red blood cells (RBCs), peripheral blood lymphocytes (PBLs), and myelogenous leukemia tumor cells (K562). Raman measurements gave unique and clear spectra for each type of cell used. This approach consists in a label-free method in which cells are analyzed continuously one-by-one by taking advantage of the Raman spectroscopy technique in order to get information about the structure of the sample at a subcellular level. The experiments are conducted at a temperature of 25°C.

2.1 Materials

Blood is provided by a healthy donor and it is placed in a phial with ethylenediaminetetraacetic acid (EDTA) in order to avoid its coagulation. Then it is diluted with a phosphate buffered saline (PBS) solution and processed in a centrifuge (Eppendorf centrifuge 810R) so that RBCs can be separated and collected from the whole blood. PBLs are obtained from healthy donors buffy coats by Ficoll–Paque density gradient centrifugation. Blood samples obtained from patients are covered by the University Magna Græcia of Catanzaro ethical approval protocol 49/CE 23072002. K562 were grown at 37 ° C in a humidified 5% CO 2 atmosphere and maintained in MEM supplemented with 10% FBS, penicillin (100 IU mL^{-1}), and streptomycin (100 μ g mL^{-1}). All products used to fabricate the microfluidic devices are purchased from commercial suppliers. For the chip, calcium fluoride slides 20 mm x 20 mm are purchased from Crystran Ltd and the dry photoresist SY330 (having a thickness of 30 μm) is purchased from ElgaEurope along with its developing and rinsing reagents. For the device interface, polymethylmethacrylate (PMMA) slides (6 mm thick and 3 mm thick) are purchased from Röhm Italia Srl. For the gaskets used in the fluidic interface, polydimethylsiloxane Sylgard 184 (PDMS) is purchased from MicroChem. Rodhamine (R6G) is purchased from Sigma Aldrich and used to characterize the enhancement factors of the nanodimers.

2.2 Working mechanisms of the Raman flow cytometer

Schematically, the channels are divided into four main areas, which are illustrated in Fig. 1 along with the schematic representation of the working principle of the device. The inlet [I] and outlet [O] of the micro channels are located at the side of the device. In the middle of the micro channel, the microfluidic trap [T] is located in which the cell can be trapped for a certain amount of time such that Raman analysis can be performed on a retained cell. The trap is realized by fabricating a constriction in width along the channel [C]. It has been designed in a way that the cell is only temporarily trapped. A dynamic change of the flow conditions are responsible for the cell entrapment. When a constant flow rate is applied a cell is moved toward the trap. When the cell is stopped at the constriction, the fluidic resistance increases accordingly and since the flow rate is constant, the pressure drop increases locally. The

#252075 Received 16 Oct 2015; revised 26 Nov 2015; accepted 27 Nov 2015; published 11 Dec 2015

increase in pressure increases the forces acting on the cell surface and this provokes a cell deformation which allows the same cell to move through the trap continuing its motion in the channel. After that, another cell approaches the trap. The role of the trap is to stop the cell for a well defined amount of time necessary to record the Raman Spectrum which can be executed in about 3 seconds. In such a way, it is possible to perform a continuous analysis of cells by Raman Spectroscopy in a passive way.

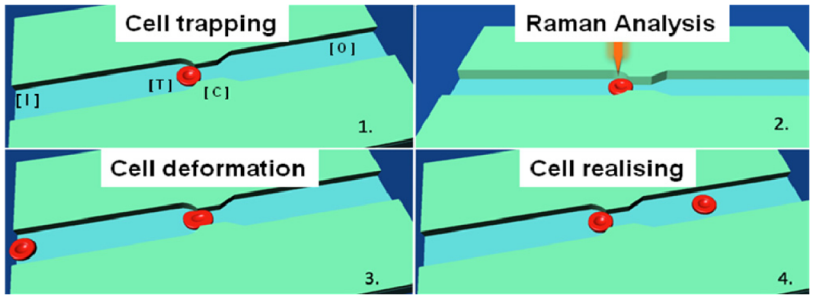

Fig. 1. Schematic representation of the microfluidic device working principle: 1. Cell trapping: [I] represents the inlet; [T] represents the position of the trap; [C] represents the constriction in width of the channel; [O] represents the outlet; 2. Raman analysis: Raman laser hits the plasmonic nanodimers where the cell is trapped and the Raman spectrum of the cell is recorded; 3. Cell deformation: The pressure deforms the cell that moves towards the constriction; 4. Cell realising: The cell passes the constriction and another cell is trapped.

2.3 Device fabrication

The microfluidic pattern containing five channels with specific shapes and sizes is sketched by using AutoCAD. The drawn pattern is loaded into a direct laser writer (DWL2000 Heidelberg) for fabricating a photolithographic chromium-glass mask which is used to fabricate the micro channels. The substrate on which the microfluidic channels are fabricated is a calcium fluoride (CaF_2) slide with a side length of 20mm and it is 0.5mm thick. After the substrate is cleaned with isopropyl alcohol (IPA) and dried with gaseous nitrogen, a dry photoresist is laminated on top of it. Once the lamination is completed, the photoresist is structured by means of photolithography. It is placed in contact with the mask and it is exposed to UV light in a mask aligner system (Karl Suss MA45). The appropriate value for exposure dose is found to be 35 seconds (with exposure energy of 250 mJ/cm^2). Subsequently the resist is baked for two minutes after exposure, developed in Ordyl SY300 developer for 4 minutes and rinsed in Ordyl SY300 rinse for 30 seconds. After the fabrication of the microfludic layout, the plasmonic nanodevices are fabricated on top of the CaF2 substrate. The nanodevices consist of gold dimers constituted of two circles of about 100 nm in diameter having a gap of 10 nm between each other. These devices are fabricated by using a FEI Nova Nanolab 600 dual beam system. The dimers are grown using electron beam induced deposition from a gas precursor containing a platinum–carbon polymer (CH3)3Pt(CpCH3). A matrix of nanodimers with a pitch of 2 μm delimited in square of 20 μm in side are fabricated by setting the electron acceleration at 30 keV and the current at 0.15 nA, then sputtered with 20nm of gold and ion beam milled. Subsequently, another slide of calcium fluoride is bonded on top of the fabricated micro channels. The bonding is obtained by using a hot press (PO Weber) and a mold where all the parts composing the device are aligned together. Different tests were performed at different temperature and pressing force, analyzing the percentage of bonded area between the different slides of the device to optimize the boding process. For the device interface, a fluidic gasket is fabricated by casting polydimethylsyloxane (PDMS) in a micromilled Polymethylmethacrylate (PMMA) mold. In particular, 2 grams of curing agent and 20 grams of silicone elastomer are mixed together. The mix is poured into the mold and degassed under vacuum. After 30 minutes, the mold is placed in an oven for 3 hours at 180°C to speed up the polymerization of PDMS. The gaskets

#252075 Received 16 Oct 2015; revised 26 Nov 2015; accepted 27 Nov 2015; published 11 Dec 2015

act as pockets in which the chip can be fixed, aligned and positioned. In fact, the gaskets integrate holes aligned in correspondence of inlets and outlets of the channels in the chip. Subsequently an external frame is fabricated in a 6mm thick PMMA slide by mechanical milling. The external frame integrates holes to accommodate external metal needles which are fixed with epoxy resin to the external frame and match with the holes in the gaskets [38]. The external frame allows to press the gaskets on the microfluidic device by means of external screws [Fig. 2]. The design of the device and the interface is such that the needles, the holes in the gaskets and the inlets and outlets result aligned. Teflon and silicone tubes are used to connect the needles to the syringe pump system. The syringe pump system allows setting the flow rate of the injected sample.

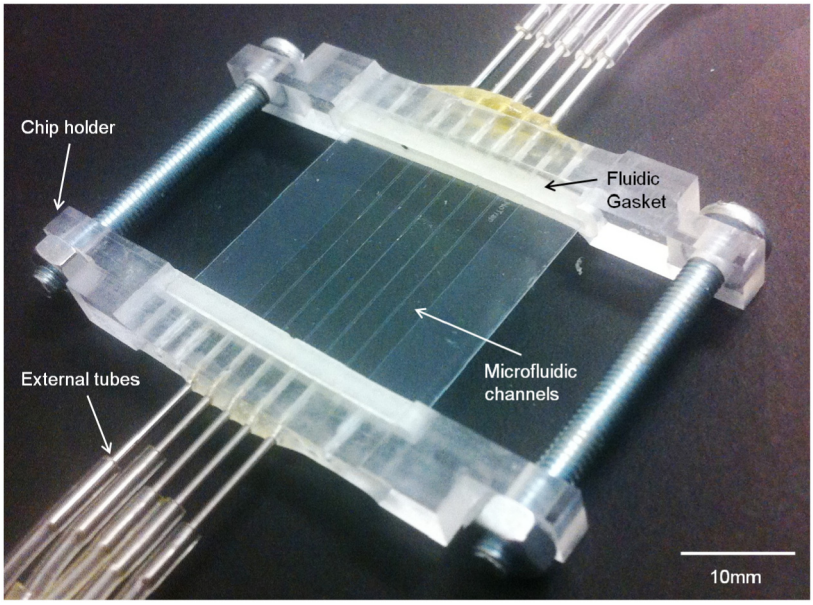

Fig. 2. Assembled microfluidic device.

2.4 Raman set-up and microfluidic protocol

The instrument used to perform Raman spectroscopy on the cells is a Renishaw inVia Raman Microscope where a 50X objective is mounted. The syringe pump (from Harvard Apparatus) system is connected to the microfluidic device by Teflon tubes (0.4mm ID) and positioned vertically close to the Renishaw to keep the syringe in a position which avoid the settling of the sample in the syringe walls. The Raman flow cytometer is located in the corresponding sample support area of the Renishaw Microscope. After the device, the interface, the tubes and the syringe pump are assembled together, 1 ml of the biological sample containing the cells diluted at a concentration of about 5000cells/μl in PBS is inserted into a 1ml syringe. The syringe is then placed into the syringe pump system such that the injection can be controlled. The flow rate is set at 5 µl/min. For the measurements, a laser with a near-infrared wavelength (832 nm) is chosen. Once the microscope is focused on the cell close to the microfluidic trap, any possible source of light is switched off so that it does not interfere with the Raman laser. The power used to analyze the sample is 10 mW and the signal collection time is 3 seconds which was found to be a suitable time for the Raman measurements. Measurements are taken on cells trapped on top of the nanodimers and compared to measurements on a flat surface to proof the enhanced Raman signal recorded on the nanodimers. Finally, measurements on RBCs, TCs, and PBLs are shown which are the averages from the signal recorded from 10 cells of the same type. We show the average spectra of 10 cells to obtain a typical spectrum of a specific type of cell comparable with the

#252075 Received 16 Oct 2015; revised 26 Nov 2015; accepted 27 Nov 2015; published 11 Dec 2015

data present in literature. In fact, a single SERS measurement is very localized and shows only a partial information about the cell and in particular of the cell membrane. In standard Raman Spectroscopy, even using a high NA objective, measurements on cells show information, not only about the cell membrane but also about the cell cytoplasm.

3. Results and discussion

3.1 Device characterization

The sizes and the shape of the channels in the chip are chosen such that the passage of the cells through the microfluidic trap can provoke a change in pressure of the flowing fluid. Pressure increases when the cell is trapped and this leads to the deformation and the movement of the cell towards the constriction. Once the cell is released the so-formed variation of pressure leads to the positioning of the following cell in the trap. Channels of different dimensions are realized in the chip in order to test which size better fits the size of the cells. This is a necessary step since photolithography has a resolution limited by diffraction down to a size of about 1 μm, which is the same order of magnitude of the trap. The microfluidic traps used for experiments on the cells have a constriction width of 8 micrometers (used for the RBCs) and 10 micrometers (used for the TCs and WBCs). This width is crucial for trapping the cells, a larger constriction will not allow the cell trapping which continue to flow, a smaller constriction will trap the cell but they will block the channels. The optimal size of the constriction was found experimentally. Another important parameter is the height of the channel, this is approximately around 11-13 micrometers after the bonding which is around the size of the cell, this ensures a contact between the cells and nanodimers. Moreover, choosing the appropriate materials for the fabrication processes of each piece composing the Raman flow cytometer device is crucial for performing proper measurements. Materials have to be durable, well suitable for the desired context and fully functional for the role they have to cover. For such a purpose calcium fluoride is chosen to fabricate the chip since it gives a negligible background signal during Raman analysis and does not interfere with it. The use of the dry resist and the lamination process has been appropriate for the resulting uniform resist layer obtained in comparison to a liquid resist that would have been spun on the substrate, leading to a more stable bonding of the lid [39]. Optical images and Scanning Electron Microscope (SEM) images of the micro channel after photolithography are shown in Fig. 3-4. Figure 3(a) shows an image of a microfluidic device after the bonding. The SEM images (Fig. 4) show in particular the layout of the microfluidic trap. Figure 3 illustrates some results of the bonding between the developed SY330 dry resist and the calcium fluoride lid. Several experiments, reported in Fig. 3(c), are conducted in order to reach the desired parameters for a suitable hot bonding technique varying the temperature from 60°C to 180°C, the applied force from 1.50 kN to 3.50 kN and the time from 2 to 5 minutes. The visible bonded area is evaluated with help of optical microscopy by making a difference between bonded and not-bonded areas (some not-bonded areas are shown in Fig. 3(b)). The best results are achieved when the sample is bonded at 180°C and by applying a force of 2 kN for 3 minutes. Even if some not-bonded areas are observed outside the channels [Fig. 3(b)], these do not interfere with the working mechanism of the device. In fact, a magnification of the channel in Fig. 3(b) demonstrates that, despite the marginal not-bonded areas, the channel is sealed and the microchannel structure is maintained.

#252075 Received 16 Oct 2015; revised 26 Nov 2015; accepted 27 Nov 2015; published 11 Dec 2015

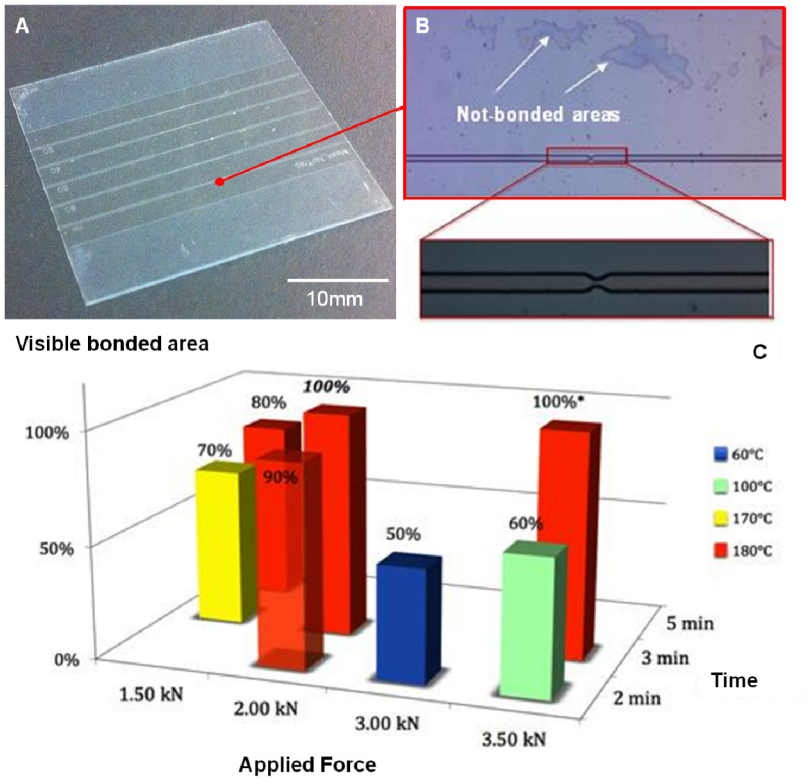

Fig. 3. (A) Optical image of an assembled microfluidic chip; (B) a channel in which a small not-bonded area is present; the magnification of (B) depicts a defined bonded channel ready to accommodate cells. (C) bonding tests results: The *x-axis* and *y-axis* report, respectively, the applied force and the time used in the tests; the different colors represent different bonding temperatures; on the *z-axis* the percentage of the bonded area is shown (100%* indicates that even if the channels are bonded they collapse, 100% is the value for a correct bonding).

3.2 Characterization of the nanodevices

In Fig. 4, it is possible to see a scanning electronic microscopy (SEM) picture of the array of 100 nanodimers fabricated in the trapping region. These have a pitch of 2 μm and are delimited in square of 20 μm in side. Each nanodevice is made of a dimer covered by a thin gold layer (20 nm). A large enhancement of the electromagnetic field is produced at the gap of the dimers, thus producing an enhancement of the Raman signal of biomolecules close to the gap [33]. During Raman measurements the objective focus is at the level of the dimer gap in order to fully exploit the signal enhancement. The dimension of the gap approximately 10 nm ensures high enhancement factors and high spatial resolution for Raman measurements [34]. In particular measurements performed by using Rodhamine at a concentration of 10^{-4}M on a flat surface and on the fabricated nanodimers showed an enhancement factor on the nanodimers of around 3.5×10^{6} in respect to the flat surface (data not shown).

#252075 Received 16 Oct 2015; revised 26 Nov 2015; accepted 27 Nov 2015; published 11 Dec 2015

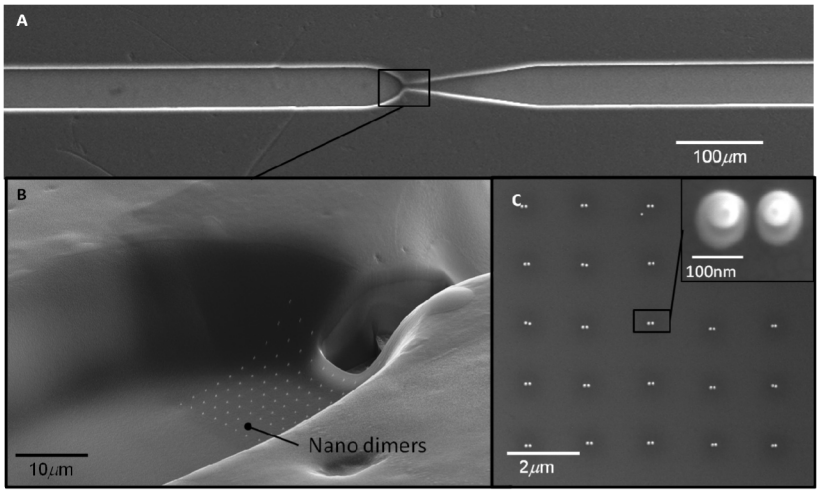

Fig. 4. Scanning electron image of the microfluidic trap and the integrated array of nanodimers. (A): Top view; (B): isometric view; (C): zoom in the area where the nanodimers are integrated.

3.3 Raman spectroscopy analysis on trapped cells

The flow rate is set at 5μl/min so that the cells can proceed very slowly and can be stopped in correspondence of the trap. In this way, Raman measurements can be performed on the cells. As shown in Fig. 5, the cells appear under the microscope and they flow one-by-one due to the well defined size of the channel which constrains them and avoid the agglomeration. This is a suitable result, ideal for the fabricated device aiming to a continuous analysis of single cells. Experiments are performed measuring the Raman spectrum of RBCs by using the microfluidic device integrating the nanodimers and a flat surface. While the measurements taken on a flat substrate need a laser power of 100% (100mW) to record a consistent spectrum, only a power of 10% (10mW) is needed to obtain an enhanced spectrum on nanodimers. This is a very important point to consider when dealing with living biological samples since a high laser power can affect the viability of the cells.

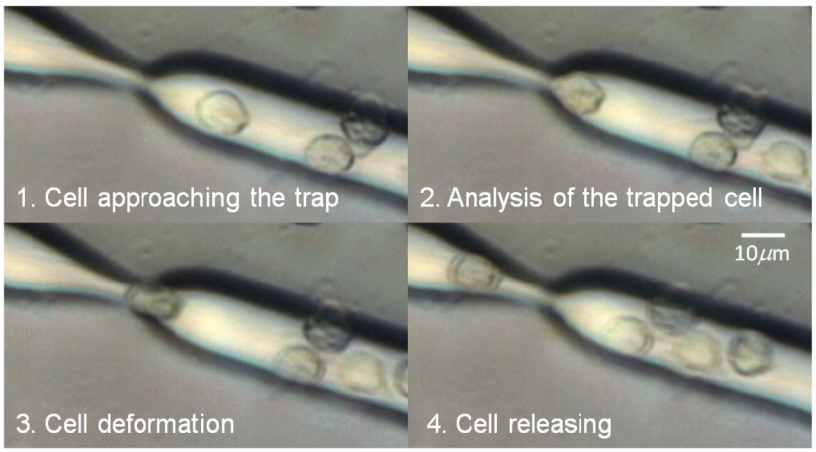

Fig. 5. Sequence of the cell analysis mechanism: (1) the cell approaches the trap followed by other cells (t = 0s); (2) the cell is trapped and the flow is stopped (t = 2s), in this phase Raman measurements can be performed on the cell (t = 4s); (3) the increasing pressure due to clogged channel deform the cell forcing it through the trap (t = 6s); (4) the cell is released continuing to move over the trap while other cells are approaching the trap aligning themselves to it (t = 8s).

#252075 Received 16 Oct 2015; revised 26 Nov 2015; accepted 27 Nov 2015; published 11 Dec 2015

In Fig. 6, it is possible to see SERS measurements which are taken on RBCs and compared with measurements taken on a substrate without nanodimers. The SERS spectrum shows not only a higher signal, compared to standard Raman, but above all the curve exhibits a richer peak profile due to plasmon-enhancement of biomolecular vibrations occurring at the dimers locations.

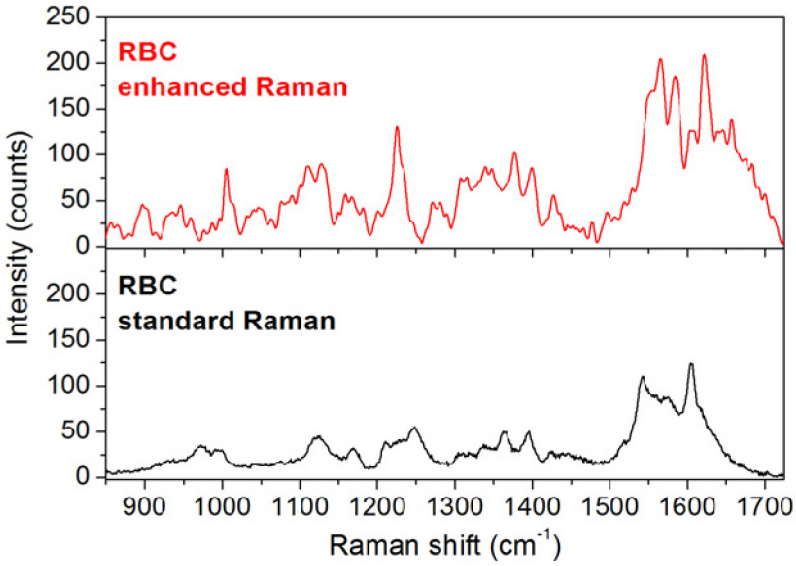

Fig. 6. Raman spectra collected from red blood cells (RBC) on nanodimers (used power for the enhanced Raman measurements is 10% of the total) and on a flat substrate (used power for the standard Raman measurements is 100% of the total). The spectrum recorder on nanodimers exhibits an higher signal and is more resolved.

Moreover, three experimental series are performed with different cell lines, and Raman spectra are collected over cells in correspondence of the trap. The used testing samples are red blood cells (RBC), peripheral blood lymphocytes (PBL) and K562 tumor cells from leukemia. Figure 7 shows the recorded Raman spectra, where each curve is the average of 10 cells acquisitions. From top to bottom we have respectively the RBC (red curve), PBL (black curve) and K562 (blue curve). The main peaks of all the three cell lines are correctly found in the Raman measurements. Concerning the red blood cells we have the typical Raman peaks of phenylalanine at 1005cm^{-1}, the deformation of the C_m-H bond at 1225cm^{-1}, the half- and quarter-ring stretching of pyrimidine respectively at 1377 and 1397cm^{-1}, and finally several peaks of the multi-structured band between 1540 and 1630cm^{-1}. As already reported in literature [40], we can observe the 1565cm^{-1} peak of the $C_\beta C_\beta$ stretching, the one at 1582cm^{-1} of $C_\alpha C_m$ asymmetric stretching, and the 1621cm^{-1} peak of $C_a = C_b$ stretching. The relative intensities of these peaks show that the RBCs are in an oxygenated state [40].

Raman signature collected on peripheral blood lymphocytes is shown in the following curve. The most evident bands are due to deoxyribose vibrations, at 980 and 1448cm^{-1} [41], to phospholipid C-C stretching at 1067cm^{-1}, and Amide I vibration from proteins secondary structure at 1665cm^{-1}. The 1448cm^{-1} peak is a broad one since it is the overlapping of deoxyribose signature with C-H deformation from proteins.

Finally the last curve shows the Raman signal coming from K562 cells. Comparison with data from the literature shows a very good agreement. As reported in [42,43] the phenylalanine ring mode at 1003cm^{-1} is observed, the PO^{2-} backbone vibration arises at 1095cm^{-1}, Amide III vibrations from proteins are located at 1203 and 1303cm^{-1} where the former one (1203cm^{-1}) overlaps with DNA bases signal, C-H bending and deformation are

#252075 Received 16 Oct 2015; revised 26 Nov 2015; accepted 27 Nov 2015; published 11 Dec 2015

respectively found at 1261 and 1448cm^{-1}, small DNA signal is also observed at 1578cm^{-1}, and finally the Amide I strong vibration from proteins is located at 1658cm^{-1}. Compared to PBL, the Amide I shift towards lower frequencies (from 1665 to 1658cm^{-1}) is likely due to a larger presence of alpha helix structure of proteins. This is also supported by the small peak observed at 935cm^{-1} (alpha helix C-C skeletal mode) for the K562 curve.

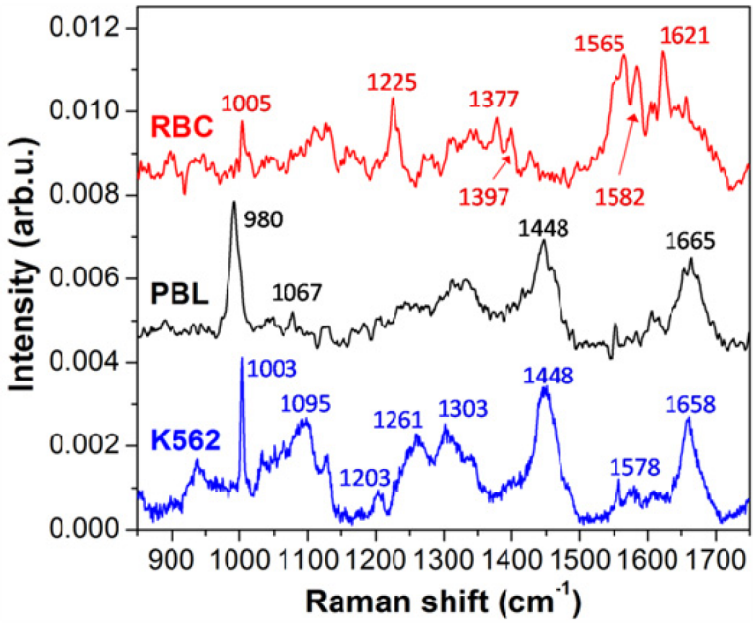

Fig. 7. Raman spectra collected in three different experiments with different cell lines, in the proximity of the microfluidic traps. From top to bottom average spectra of red blood cells (RBC), peripheral blood lymphocytes (PBL), and K562 tumor cells from leukemia are reported. See the text for assignment of the main peaks.

4. Conclusions

The proposed microfluidic device integrating plasmonic nanodimers used in combination with Raman Spectroscopy t is a fast method to look at single cell in a complex multicellular sample. The design and the chosen materials proved to be suitable for the aim of this work. The Raman flow cytometer was used to analyze single red blood cells, lymphocytes and myeloma tumor cells and the resulted Raman measurements found correspondence with those presented in literature. Thanks to further optimization, this device will potentially become a fast cell by cell diagnostic tool with an amount of information that other optical techniques are lacking.

Acknowledgments

This work was partially supported by the European project EUROMBR (grant no. 608104), Cariplo Foundation under the project "New Frontiers in Plasmonic Nanosensing" (Grant no. 2011-0338), the project for Young researchers financed from the Ministry of Health "High Throughput analysis of cancer cells for therapy evaluation by microfluidic platforms integrating plasmonic nanodevices" (CUP J65C13001350001, project no. GR-2010-2311677) granted to the nanotechnology laboratory of the Department of Experimental and Clinical Medicine of the University "Magna Graecia" of Catanzaro.

#252075 Received 16 Oct 2015; revised 26 Nov 2015; accepted 27 Nov 2015; published 11 Dec 2015